Aquacultural Engineering xxx (xxxx) xxx

Contents lists available at ScienceDirect

Aquacultural Engineering

journal homepage: www.elsevier.com/locate/aque

Corrigendum

Corrigendum to "Automatic detection of fin, operculum, and skin deformities in Mediterranean fish species" [Aquac. Eng. 113 (2026) 102684]

Ioannis Christofilogiannis [a,b], Dimitra G. Georgopoulou [a,*], Charalabos Vouidaskis [a], Zacharias Choulakis [a], Dimitris Voskakis [a], Nikos Papandroulakis [a,*]

[a] Institute of Marine Biology, Biotechnology and Aquaculture (IMBBC), Hellenic Centre for Marine Research (HCMR), Heraklion, Crete, Greece
[b] AQUARK, Aquaculture Consultants, Zografou, Greece

The authors regret an error in the published article regarding author affiliations.

In the originally published version, the affiliation "[a]Institute of Marine Biology, Biotechnology and Aquaculture (IMBBC), Hellenic Centre for Marine Research (HCMR), Heraklion, Crete, Greece" was incorrectly attributed to the first author, Ioannis Christofilogiannis. This affiliation should be removed from the first author's details.

This correction does not affect the scientific content or conclusions of the article.

The authors would like to apologise for any inconvenience caused.

DOI of original article: https://doi.org/10.1016/j.aquaeng.2025.102684.
* Corresponding authors.
E-mail address: d.georgopoulou@hcmr.gr (D.G. Georgopoulou).

https://doi.org/10.1016/j.aquaeng.2026.102704

Aquacultural Engineering 113 (2026) 102684

Contents lists available at ScienceDirect

Aquacultural Engineering

journal homepage: www.elsevier.com/locate/aque

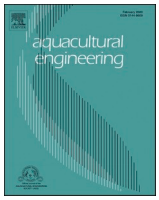

Automatic detection of fin, operculum and skin deformities in Mediterranean Fish Species

Ioannis Christofilogiannis [a,b], Dimitra G. Georgopoulou [a,*], Charalabos Vouidaskis [a], Zacharias Choulakis [a], Dimitris Voskakis [a], Nikos Papandroulakis [a,*]

[a] Institute of Marine Biology, Biotechnology and Aquaculture (IMBBC),Hellenic Centre for Marine Research (HCMR), Heraklion, Crete, Greece
[b] AQUARK, Aquaculture Consultants, Zografou, Greece

ARTICLE INFO

Keywords:
Finfish aquaculture
Fish welfare
Morphological abnormalities
Computer vision
YOLO
Underwater imaging
European seabass
Gilthead seabream

ABSTRACT

Morphological deformities in farmed fish can significantly impair swimming performance, feeding efficiency, and overall welfare, leading to economic losses in aquaculture. In this study, we apply deep learning-based computer vision models to automatically detect pectoral and caudal fin deformities as well as skin and operculum deformities ("red spots") in two key Mediterranean species: European seabass (*Dicentrarchus labrax*) and gilthead seabream (*Sparus aurata*). Using underwater stereo-vision imagery from our pilot-scale fish farm, we developed diverse annotated datasets for each morphological feature through a combination of manual labeling, an AI-assisted annotation tool and data expansion pipelines (data augmentation). We trained and evaluated multiple computer vision model architectures to address underwater imaging challenges such as motion blur, occlusion, and variable light intensities. Across all model comparisons, the lightweight YOLOv12s model achieved the best balance of accuracy and computational efficiency, with mean Average Precision values up to 0.81 for fin classification and 0.91 for red spot detection, while enabling real-time inference. Our results demonstrate that small CNN models, improved with attention-based methods like the YOLOv12s and trained on diverse, well-prepared images, can assess fish morphology in real aquaculture environments. This approach offers a scalable, non-invasive monitoring solution to support real-time monitoring and early health interventions and improve fish welfare in intensive farming systems.

1. Introduction

In recent years, aquaculture has become a major contributor to the global supply of fishery products, providing around 60 % of the fish for human consumption (FAO, 2024). In 2023, global fishery production reached 136.17 million tonnes with a first-sale value of 292.78 billion euros, reflecting increases of 3.7 % in volume and 4.3 % in value compared to the previous year (HAPO, 2025). While Asia dominates aquaculture output, the European Union remains an important producer, with 558,615 tonnes valued at 2.89 billion euros in 2023 (HAPO, 2025). Within the EU, gilthead seabream (*Sparus aurata*) and European seabass (*Dicentrarchus labrax*) are among the most economically significant species, ranking third and fifth in production volume, respectively. Together, they represent 35 % of total EU aquaculture fish volume and contribute over 1 billion euros in first-sale value, with European seabass valued at 544.5 million euros and gilthead seabream at 500.7 million euros (HAPO, 2025).

High product quality and animal welfare has become increasingly important for the sustainable growth of Mediterranean mariculture. However, morphological abnormalities pose a persistent challenge to these goals. Extensive studies in farmed species (Branson, 2008; Koumoundouros, 2010; Noble et al., 2012) resulted in several causative factors, such as genetics, nutritional, poor handling practices, environmental contaminants, water temperature, hypoxia and variable rearing conditions that contribute to the incidence of abnormalities (Divanach et al., 1996; Chandra et al., 2024; Noble et al., 2012). Either malformations, i.e structural deviations caused by intrinsic errors and genetics in early development or deformities i.e. changes in shape from external mechanical forces (Dygut and Piwowar, 2025), the majority of these abnormalities are developed during the early larval stages and therefore are eliminated at the hatcheries, by sorting, before fish are transferred to cage for on-growing. However, deformities of the fins or skin, can develop also during the on-growing activities as a result of poor husbandry practices representing main operational welfare indicators for

* Corresponding authors.

https://doi.org/10.1016/j.aquaeng.2025.102684
Received 17 September 2025; Received in revised form 15 December 2025; Accepted 18 December 2025
Available online 26 December 2025

finfish farming (Noble et al., 2026).

Fin integrity is widely recognized as both a sensitive and reliable indicator of fish health and welfare. The caudal and pectoral fins, are of particular concern due to their central role in swimming, feeding, and maintaining spatial orientation (Lauder, 2000; Thorsen and Westneat, 2005; Westneat et al., 2004). The caudal fin serves as the primary propulsive organ during locomotion (Lauder, 2000), while the pectoral fins, located behind the operculum, are paired appendages essential for maneuverability, posture stabilization, and precise movement control (Westneat et al., 2004). Fin deformities may range from erosion and frayed edges to complete separation between fin rays or deviations from normal fin morphology, such as loss of the characteristic triangular shape (Smith et al., 2002). Damage to either fin type may impair swimming ability, feeding efficiency, may increase susceptibility to infection and ultimately affect growth and survival (Noble et al., 2012; Chandra et al., 2024). From a production perspective, fin damage seems to reduce the market value of an affected individual (Noble et al., 2012). Although studies have examined the effects of fin clipping across various species, despite the pectoral fin's biomechanical and behavioral significance, it remains an under-investigated anatomical feature in fish health assessments—particularly in key commercial species such as E. seabass and g. seabream (Mhalhel et al., 2023). Regarding causative factors, caudal fin deformities could be attributed to high stocking density (Jeannine and Bayon, 2009), cannibalism (Hatziathanasiou et al., 2002), congenital skeletal malformations (Hennekam et al., 2013), or acquired skeletal deformations (Boglione et al., 2014; Kourkouta et al., 2024). Caudal fin erosion could also be attributed to water quality coupled with stress and bacterial secondary infection e.g. *Tenacibaculum* spp (Gourzioti et al., 2018). As aquaculture expands, there is an increasing need for rapid, objective, and scalable tools to assess such deformities and improve production outcomes.

Skin integrity is also very important in fish, as it is the physical barrier that can protect the fish from various infections (Yun et al., 2021). Skin rashes and skin lesions can therefore be a direct or indirect sign of poor rearing conditions or underlying diseases caused by bacterial or viral infections. There are several skin pathologies present in marine species in the Mediterranean sea, for example the red spot disease in sole (*Solea spp.*, Flüchter 1979), ulcerative dermatitis in dusky grouper (*Epinephelus marginatus*, Rizgalla et al. 2016) and the petechial rash (PR)/red spot disease (RSD) in g. seabream and E. seabass (Schmidt et al., 2018). Skin lesions on the side of the body and on the caudal peduncle of the caudal fin start as abrasions or loss of scales and shallow wounds with focal petechiae and haemorhage due to overstocking, low water quality or infectious pathology (Sveen et al., 2020, Lévesque et al., 2013).

Operculum deformities, such as operculum folding, are common skeletal abnormalities in cultured fish, involving the opercular and subopercular bones and appearing as uni- or bilateral malformations of the gill cover (Koumoundouros et al., 1997; Verhaegen et al., 2007; Ortiz-Delgado et al., 2014). It can be caused by multiple factors like nutritional imbalances, genetic factors, environmental stressors such as stocking density and water conditions, and mechanical influences (Boglione et al., 2013; Koumoundouros, 2010; Witten & Huysseune, 2009). Opercular deformities reduce respiratory efficiency by exposing the gills, increasing susceptibility to hypoxia and parasite infections, and are often associated with reduced biological performance and welfare (Paperna et al., 1980; Beraldo et al., 2003) and in most of the cases the majority of the deformed individuals are eliminated at the hatchery level. From a commercial perspective, these deformities negatively affect fish appearance, lowering market value and consumer confidence in aquaculture products (Noble et al., 2012). Therefore, monitoring opercular deformities is essential for improving fish welfare, optimizing farming practices, and maintaining product quality in aquaculture systems.

Generally, there is significant research interest on fish morphology assessment, spanning from manual morphometric measurements to automated, AI-driven biometric analysis (Yu et al., 2021; Li et al., 2022; Liu et al., 2023; Kumar et al., 2023) and from embryos (Naudin et al., 1996; Teixidó Condomines et al., 2019) to juveniles (Kvæstad et al., 2022; Nikolakakis et al., 2014; Bellis et al., 2024) and adult fish (Feng et al., 2025). These studies differ in variable aspects, such as the type of detected abnormality, the species used, the algorithmic approach and the application conditions (laboratory vs farming conditions).

Chronologically, the field has evolved from low-cost early detection approaches to advanced, non-invasive machine-learning frameworks enabling automated detection. Early work relied on simple image analysis and manual interpretation (Naudin et al., 1996; Boglione et al., 2014; Sun et al., 2009) that later progressed to rule-based computer--vision pipelines and classical machine learning (ML) classifiers (Teixidó Con-domines et al., 2019; Costa et al., 2013). Techniques such as microradiography provided high-resolution skeletal assessment but still rely heavily on expert manual scoring and manually placed landmarks (Pousis et al., 2022). More recently, deep CNNs have enabled fully automated classification of complex developmental phenotypes and larval malformations (Čapek et al., 2023). Lightweight CNN architectures using specific key-points in the fish has also emerged, allowing automated measurements of body shape and skeletal traits ready to be applied to field trial (Luo, 2024; Saleh et al., 2023).

Research on the automatic detection of morphological deformities in adult or market-size fish remains relatively limited. Most previous efforts to characterize such abnormalities in aquaculture species have relied on manual radiographic or pathological examinations, as demonstrated in detailed analyses of vertebral deformities in Atlantic salmon (Holm et al., 2020) and comprehensive reviews of skeletal, cranial, and vertebral malformations across farmed species (Chandra et al., 2024). These approaches, however, lack the capacity for real-time and large-scale assessment under farming conditions. Vision-based sorting systems, such as those proposed by Costa et al. (2013), have incorporated external imaging, outline-based morphometry, and multivariate classification models to discriminate among size classes, sex, and skeletal anomalies in E. seabass, thereby enabling high-throughput screening of adult individuals. More recently, industrial-scale applications have begun to integrate deep learning approaches—particularly object detection and feature extraction networks—to capture detailed morphological traits in larger fish, for example on large yellow croaker (*Larimichthys crocea,* Feng et al., 2025).

Considering the above, the current study aims to develop an AI-powered, deep learning computer vision tool that will be capable of real-time automatic detection of multiple morphological deformities (pectoral and caudal fin deformities, operculum deformities and skin lesions). The tool is designed for the two most important Mediterranean aquaculture fish species, the European seabass and the gilthead seabream, under real fish farming conditions. Ultimately, the goal is to contribute toward more efficient, data-driven real-time farm welfare and health monitoring systems in aquaculture through the integration of AI-powered image analysis and annotation tools.

2. Methodology

In this section we describe how we collected the images, the characterization of the deformities and their classification, the annotation procedure and finally the analysis and classification process.

2.1. Data collection

The annotation dataset consisted of images from our pilot-scale floating net-pen cage farm, which is certified as an aquaculture facility by the national veterinary authority. Groups of gilthead seabream and European seabass of more than 10,000 individuals each (mean weight E. seabass = 358.42 ± 161.52 g, weight g. seabream = 347.32 ± 89.82 g), were reared in circular polyester cages of 40 m in diameter, consisting of a cylindrical net extending to 8 m and a conical bottom of 1 m, with an

approximate stocking density of 5.2 kg m^{-3}.

Images were captured using a custom-made underwater stereo vision camera (Voskakis et al., 2021), which is routinely employed at the farm to record footage twice a week (each sampling session lasts approximately 30 min, resulting in almost 5000 – 6000 image frames) for size estimation of both European seabass and gilthead seabream.

2.2. Data classification for annotation

Pectoral and caudal fins were classified as “Good” or “Bad” based on their particular morphological characteristics in both, the European seabass and the gilthead seabream. During the annotation process a rectangle around each morphological feature was drawn and a ‘Good” or “Bad” class was assigned to it.

The skin lesions and the operculum deformities appear with a distinct red color, i.e. a red spot. Therefore, a rectangle around each red spot was drawn to annotate the presence of this class in the image.

In the following section, the variable morphological deviations that helped us define a "Bad" pectoral and caudal fin are described and analyzed, along with the characteristics of the red spots in both species. In addition, the criteria for the exclusion of some of the features from annotation are also defined, a requirement for better training outcomes. Real examples of images with specific deformities can be found in the Appendix.

2.2.1. Pectoral and Caudal fin deformities in European seabass

The categories of European seabass pectoral fin deformities are described in Fig. 1a:

(A) Deep gradual erosion in the middle line of the pectoral fin.
(B) Fragile pectoral fin edges leading to deep longitudinal separations between fin rays.
(C) Erosion of the skin layers between fin arrays that leads to separation of major sections of the fins while the length of the fin arrays remains intact.
(D) Rounding and shortening of the edges and darkening of the color of the upper section of the pectoral fin with development of parallel longitudinal lines in the lower section.

The European seabass caudal fin deformities are described in Fig. 2a:

(A) Mechanical erosion of the top part of the caudal fin.
(B) Fragile caudal fin edges and middle line erosion.
(C) Erosion of the skin layers between caudal fin arrays that leads to total caudal fin erosion.

2.2.2. Pectoral and Caudal deformities in gilthead seabream

The gilthead seabream pectoral fin *deformities* are described Fig. 1b:

(E) Fins that have deep longitudinal incisions between rays.
(F) Fins that have frail edges, that show gradual erosion.
(G) Fin with abnormal shape due to shortening of fin rays, loss of triangular form.
(H) Fins with total separation between fin sections.
(I) Fins with significant loss of fin rays and darkened base.

The gilthead seabream caudal fin *deformities* are described Fig. 2b:

(A) Gradual middle line erosion.
(B) Fragile caudal fin edges.
(C) Mechanical erosion of the top part of the caudal fin accompanied by fragile caudal fin edges and deep longitudinal incisions.
(D) Erosion of the top part of the caudal fin and the skin layers between fin arrays that leads to total caudal fin erosion.

2.2.3. Red spots in European seabass and gilthead seabream

Red spots appear on both species at different areas of their body (indicated as A, B and C in Fig. 3).

Area (A): Deformity of Opercula leads to exposure of the gill arches. The deformity appears with a distinct “reddish” coloration in the image.

Areas (B) and (C): Red spot skin lesions on the side of the body and on the caudal peduncle of the caudal fin appear as abrasions or loss of scales

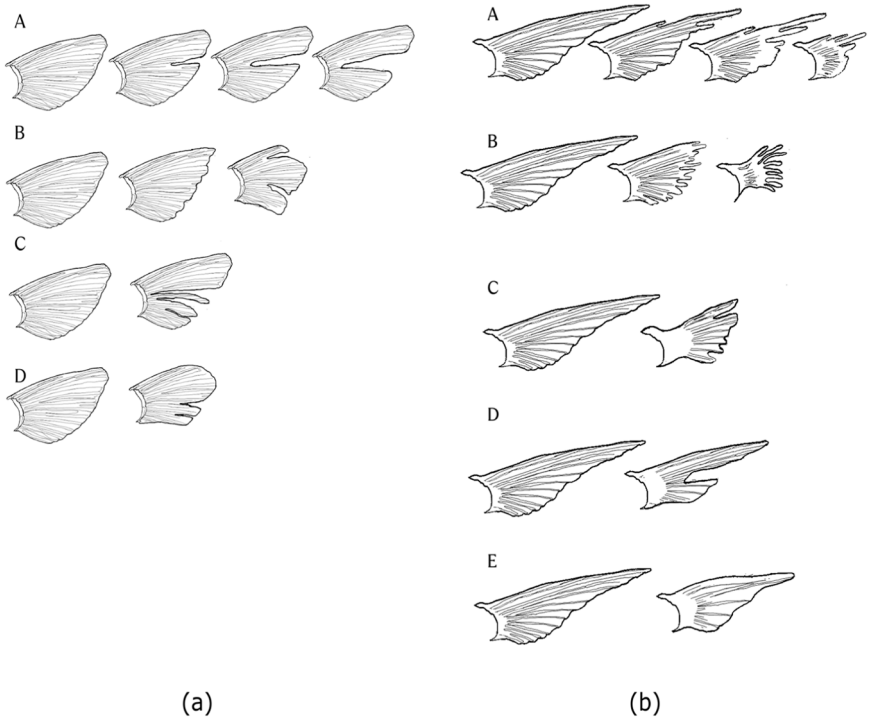

Fig. 1. Categories of deformities in pectoral fin of European sea bass (a) and gilthead seabream (b).

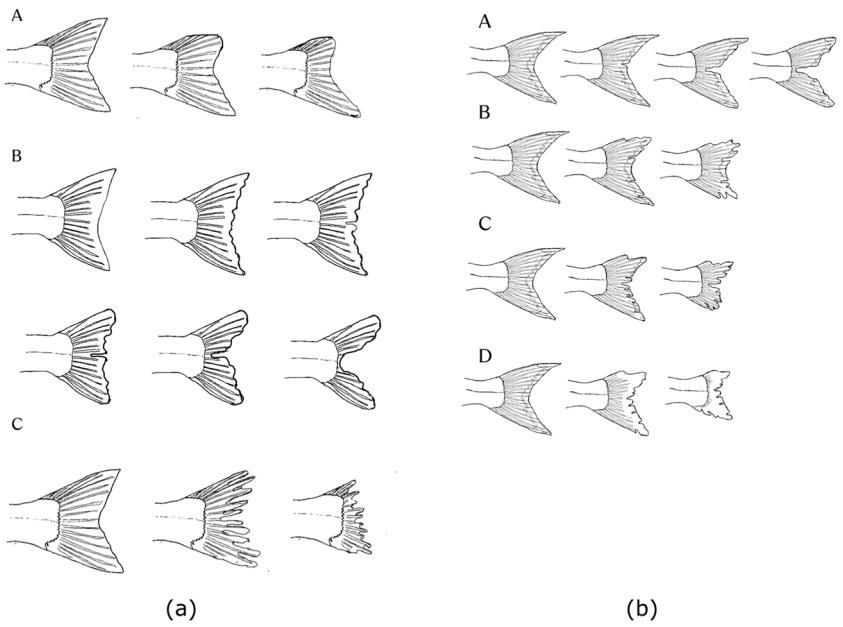

Fig. 2. Categories of deformities / lesions in the caudal fin of European seabass (a) and gilthead seabream (b).

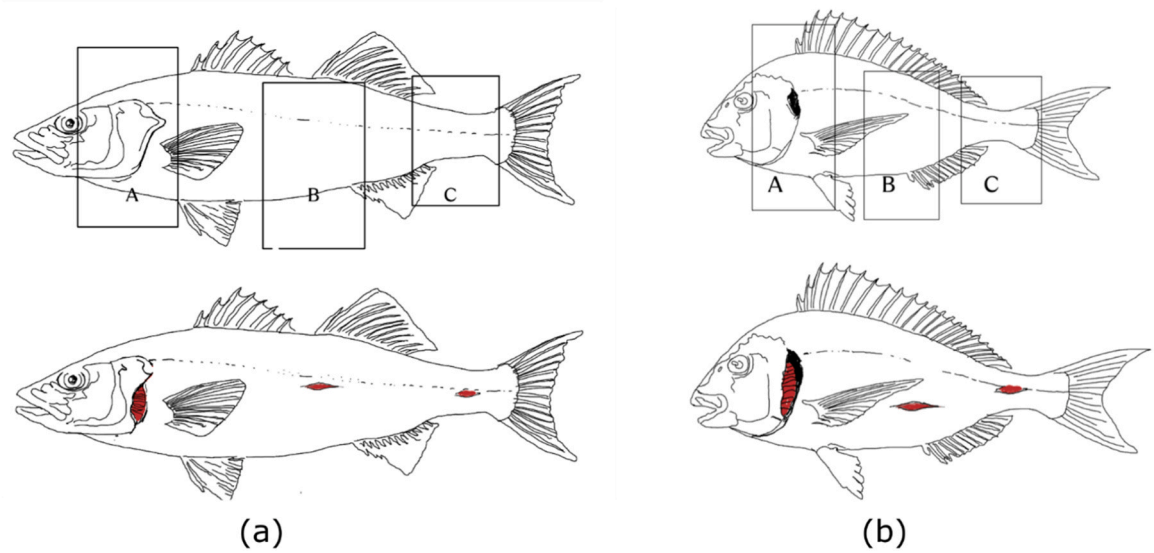

Fig. 3. Red spots detection in the European seabass (a) and the gilthead seabream (b).

and shallow wounds.

The work of Cuvier and Valenciennes (1828) and Seafish (2025) were used as a basis for tracing the normal healthy pectoral and caudal fins of g. seabream (Fig. 1b) and E. seabass (Fig. 1a) respectively as well as the fish diagrams for red spots (Fig. 3). For the fins with deformities and the red spot, representative samples of the collected underwater images were used.

2.3. Data annotation

Roboflow, a platform used to create, manage, and deploy computer vision datasets (https://roboflow.com/), was used to annotate red spots and caudal fin datasets. A custom-made Assisted Annotation Tool was developed for the classification of pectoral fins representing an efficient solution for image annotation workflows by integrating manual and AI-assisted capabilities. This PyQt6-based (https://pypi.org/project/PyQt6/) application simplifies and speeds up bounding box annotation through an intuitive interface coupled with YOLO object detection, specifically designed for binary classification ("Good fin" / "Bad fin", Fig. 4) which significantly speeds up the annotation process. The tool supports standard YOLO/Roboflow dataset structures with train/valid/test datasets, ensuring compatibility with the broader YOLO ecosystem. Workflow optimizations include keyboard shortcuts, progress tracking, and direct image navigation to accelerate the annotation process. By combining AI-assisted detection with manual refinement, the application significantly reduces annotation time while maintaining quality. The modular architecture allows easy extension beyond binary classification, making it adaptable to diverse research contexts.

The pipeline utilized in this study is described in Fig. 5. More specifically, an initial model was generated with a small number of samples and was used was used as an input in the annotation tool to generate new annotations. The annotated bounding boxes were then be manually inspected, and were accepted or deleted, and new bounding boxes also were manually added to the dataset. Finally, by tuning the augmentation

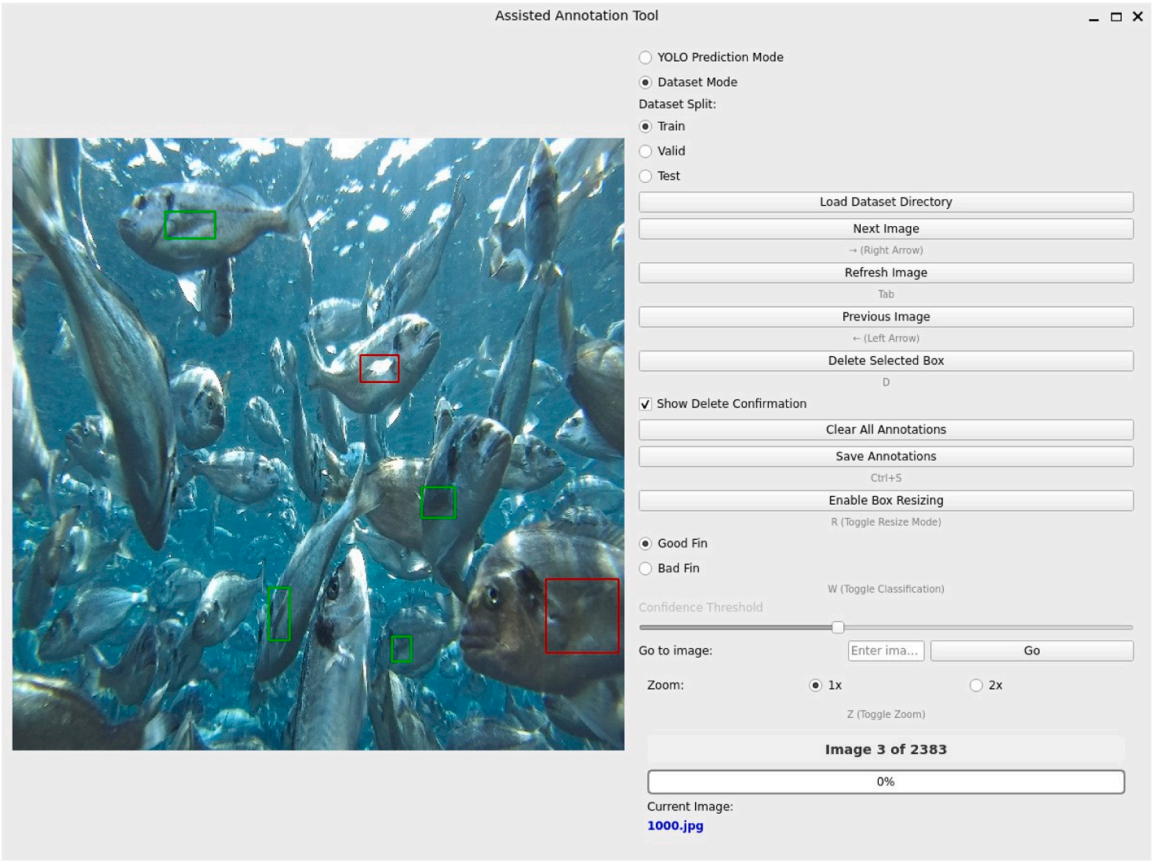

Fig. 4. Cross-platform assisted annotation tool running on Linux, displaying an image with bounding box annotations. The interface shows the canvas (left) and control panel (right) with dataset navigation, annotation controls, and zoom options. Green annotation represents a good fin class and red annotation a bad fin class.

parameters, testing different YOLOv12 configurations, and increasing sample size, a new more accurate model was trained. This process was then repeated using this new model as a basis for future annotations.

A pectoral or caudal fin with no visible deformities and a normal fin shape (see the criteria in 2.2) is classified into the "Good Fin" class (Green annotation). Fins that have clearly visible deformities are grouped into the "Bad Fin" class (Red annotation). In addition, red spots on the skin are annotated only based on their presence.

2.4. Augmentation strategies

To improve model generalization and therefore predictability, we applied different augmentation techniques commonly used in YOLO training. These augmentations artificially expand the training dataset by introducing controlled variations of the original images, helping the model learn invariant features across different conditions. For example, "Scale" randomly resizes images to handle objects at varying sizes, while "Mosaic" combines four images into one composite to enhance multi-scale detection across diverse contexts. "Erasing" randomly removes (masks) a rectangular region of an image and replaces it with a constant value or noise. It helps the model become robust to occlusion. "Rotation" rotates the image by a certain angle (e.g., ±10–30°). It makes the model invariant to orientation changes. Finally "Mixup" combines two images by blending their pixels and mixes their labels proportionally. Improves generalization and reduces overfitting. In our study we tested two different groups of augmentation techniques, the configuration 1 (consisting of scale, mosaic and erasing) and configuration 2 (consisting of scale, mosaic, erasing, rotation, and mixup) as seen in Table 1.

We utilized YOLOv8 and YOLOv12 architectures to test the augmentation strategies. Although YOLOv8 was our primary model, we expanded our testing to include YOLOv12 upon its release due to its superior accuracy-efficiency trade-off, which overcomes the limitations of traditional CNN-based detectors through optimized attention mechanisms (Tian et al., 2025). The two architectures were trained using the gilthead seabream dataset of the pectoral fin deformities. Classifying pectoral fins was the most challenging problem. The seabream pectoral fin dataset required the annotation of a very large number of samples to reach a high mAP50 performance, so it was the best dataset to test different augmentation configurations.

2.5. Exclusion of annotated samples

During the annotation process, we deliberately excluded certain pectoral and caudal fins from labeling due to several factors that compromised reliable identification (Fig. 6). Motion artifacts in underwater imagery frequently resulted in blurred or not distinct fins. Additionally, fins lacking characteristic morphological features were omitted to maintain annotation quality. Environmental factors also necessitated exclusions, particularly when shadow effects or occlusion by other fish obscured fin outlines. Similarly, over exposure to lighting rendered some fin boundaries not easily defined prohibiting accurate annotation. Finally, clipped fins at image boundaries were excluded to maintain annotation integrity, as these partial features would have provided inadequate training examples (Fig. 6a, b). These exclusion criteria were systematically applied to ensure the resulting dataset contained only high-confidence annotations. The exclusion task was performed by manual validation of the dataset images. The decision on whether to keep an image or not was also influenced by the annotation tool, as in some cases the YOLO models did not detect or misclassified noisy fin images, which were subsequently removed. This validation task was not time consuming as the dataset images were checked two times and after each exclusion task classification performance increased. Approximately

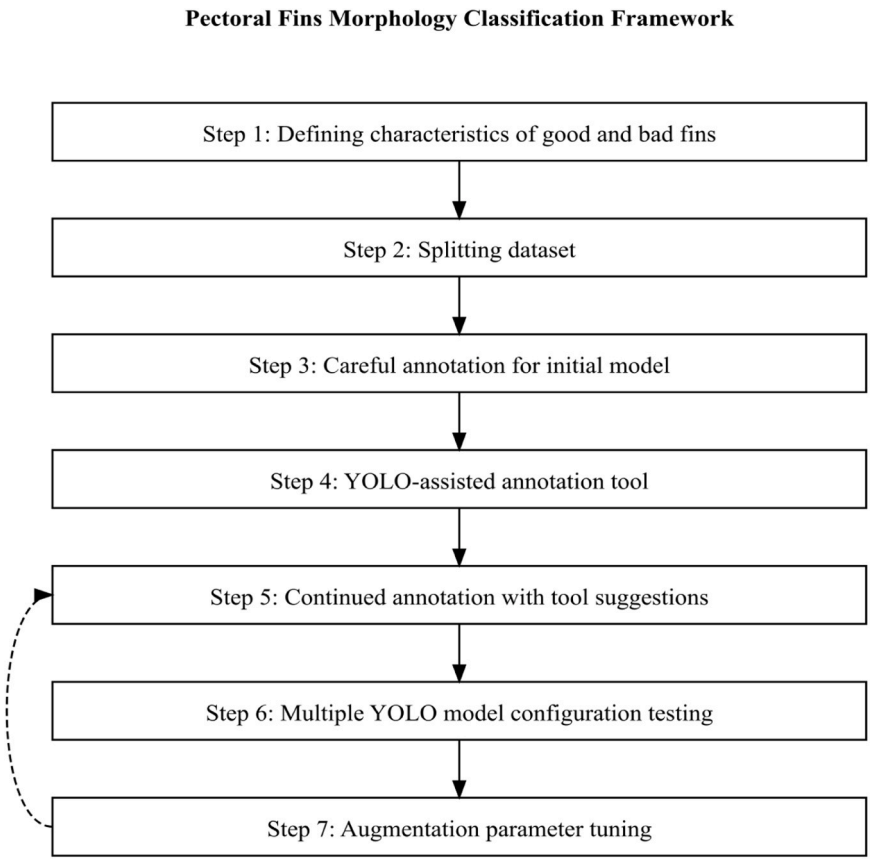

Fig. 5. Data annotation process flow using the YOLO-assisted annotation tool.

Table 1
Augmentation configurations with each parameter's value.

Techniques	Config 1	Config 2
Scale	0.4	0.4
Mosaic	0.9	0.9
Erasing	0.1	0.2
Rotation (degrees)	-	1.0
Mixup	-	0.2

15–20 % of examined images were excluded from the annotation datasets for the above reasons.

2.6. Model training performance

Model training was implemented for all morphometric characteristics in both species using the Ultralytics YOLO framework (different versions of it, i.e., YOLOv8 (Ultralytics, 2023) and YOLOv12 (Tian et al., 2025) of different sizes (YOLOv8 nano with 3.2 M, YOLOv8 large with 43.6 M parameters and YOLO12 small with 9.2 M parameters) with PyTorch backend on NVIDIA RTX 4080 GPU. Different batch sizes (typically 8–24 images) with 640 × 640 pixel input resolution were used, along with an early stopping patience of 50 epochs to prevent overfitting. The AdamW optimizer (Loshchilov and Hutter, 2017) was utilized with initial learning rate of 0.001, while augmentation strategies including Mosaic, Mixup and random Erasing were used to simulate

Fig. 6. Examples of excluded Bad fins. (a) Excluded Bad caudal fin (tail) that is covered by another fish, (b) Excluded Bad partial caudal fin (tail) in the edge of the image.

realistic underwater conditions without compromising morphology. Training employed 2074 images with two classes on an NVIDIA RTX 4080 GPU, with batch size 12, image size 640 × 640, and early stopping.

For deciding the best augmentation strategies YOLOv8 and YOLOv12 architectures were trained using the gilthead seabream dataset of the pectoral fin deformities. We chose the pectoral fin as was the most challenging problem as mentioned before in paragraph 1.4.

Although the main focus of this study was on using YOLO models, the RT-DETR large model (32 M parameters) was also tested for comparison. RT-DETR was selected for testing due to its ability to achieve real-time object detection performance, powered by its transformer-based architecture (Zhao et al., 2024).

Model evaluation used Precision, Recall, mAP50 (i.e. with IoU threshold of 0.5) and mAP50−95, and the best-performing weights were automatically selected based on validation performance. Precision (P) and Recall (R) are standard metrics used to evaluate object detection performance. Precision measures the proportion of correct detections among all predicted detections, while recall measures the proportion of true objects that are correctly detected. These metrics are calculated by comparing predicted bounding boxes with ground-truth annotations using an Intersection over Union (IoU) threshold. Mean Average Precision (mAP) summarizes detection performance by averaging the precision–recall curve across classes. mAP50 is calculated at a fixed IoU threshold of 0.50, meaning a detection is considered correct if it overlaps the ground truth by at least 50 %. mAP50–95 is a stricter metric that averages mAP values across multiple IoU thresholds, from 0.50 to 0.95 in steps of 0.05. In this study, the mAP50 evaluation metric was used as the benchmark to determine the best results.

2.7. Tracking

Detections were recorded with normalized bounding box coordinates (scaled to image dimensions) and confidence scores. To ensure consistent identification of pectoral fins, caudal fins and red spots across video sequences, multi-object tracking was implemented using the Ultralytics YOLOv8 and YOLO12 framework's built-in tracking capabilities. The tracking algorithm maintained persistent object identities by associating detections between consecutive frames based on spatial proximity and appearance similarity. Each detected pectoral or caudal fin, or red spot was assigned a unique integer identifier upon first detection, which was maintained throughout the sequence using the model.track() function with persistence enabled. This approach allowed for temporal consistency analysis, enabling the system to track the same anatomical feature across multiple frames and reducing false classifications caused by momentary occlusions or detection artifacts.

To maintain data integrity, a post-processing quality control step was implemented that identifies and removes tracking IDs. This helped us avoid exhibiting inconsistent classifications (i.e., the same tracked object labeled as both "Good" and "Bad" across different frames) or repetitive detections of deformities in the same individual at different frames. The tracking history was stored as coordinate trajectories for each identified object, with a rolling window of five frames to balance computational efficiency with tracking accuracy. When tracking failed due to occlusion or detection gaps, objects were assigned a null identifier ('none') and processed as independent detections, ensuring that untracked objects still contributed to the overall assessment while maintaining the integrity of the tracked dataset.

3. Results

3.1. Data augmentation

The use of augmentation techniques improved significantly the models. More specifically, **mAP** value of the Yolov12s model improved from 0.62 (without augmentations) to 0.73 (with configuration2 augmentations). Among the two configurations tested for creating the final annotation dataset, Configuration 2 achieved the best results ($\mathbf{mAP_{conf2}} = 0.733$ vs $\mathbf{mAP_{conf1}} = 0.729$; Table 2).

Testing with multiple configurations revealed several important insights. Mosaic augmentation (i.e., the combination of four training images into one) with probability set to 0.9 provided the best results compared to its lower values, effectively simulating varied group densities in underwater scenes.

In addition, the analysis identified several approaches that negatively impacted results. Excessive copy-paste augmentation and high Mixup values degraded model performance by creating unrealistic spatial arrangements and introducing label confusion. Conversely, random Erasing at 0.2 probability effectively simulated occlusions typical in underwater environments, thereby improving model generalization to environmental changes.

With respect to geometric transformations, with the addition of limited Rotation (1.0°) in the configuration 2 we saw a slightly improved performance while preserving the recognizable morphological characteristics of fins, which are critical for accurate identification. These findings collectively demonstrate that domain-specific augmentation strategies significantly impact underwater object detection performance, with smaller well-optimized models outperforming larger architectures when coupled with appropriate data augmentation techniques.

Table 2 demonstrates performance metrics for three model variants on the gilthead seabream pectoral fin assessment, with different augmentation configurations, including class-specific metrics for each model.

The optimized YOLOv12s configuration (Config 2) achieved the best overall metrics ($\mathbf{mAP_{50}}$ of 0.73) despite the fact that this model architecture has less than half intrinsic parameters compared to the YOLOv12m model (9.3 M vs 20.2 M).

3.2. Model training performance

The best results for the red spot dataset were achieved with RT-DETR large model with $\mathbf{mAP_{50}} = 0.89$ (Table 3). The YOLOv8 large model (Ultralytics, 2023) was second best for the red spot detection with $\mathbf{mAP_{50}} = 0.89$. However, this difference considering the model size (32 M parameters for RT-DETR vs 9.2 M parameters for YOLO12s) is not considered significant. Consequently, the YOLO12s model provided the best results for the red spot experiment, demonstrating an optimal balance between computational efficiency and detection performance relative to larger model variants from both the YOLOv8 and YOLO12 families and the RT-DETR model.

Regarding the pectoral fin dataset the small model YOLOv12 gave the best results for the gilthead seabream mAP50 = 0.73. However, in these comparisons the dataset used in YOLOv12 was also bigger (marked by * in Table 3) something that could potentially improve the metrics.

Table 2
Augmentation Testing with overall and class-specific metrics.

Model	Overall	Class Performance (Bad fin/Good fin)	
	P/R/mAP$_{50}$/ mAP$_{50-95}$	**P/R/mAP$_{50}$/mAP$_{50-95}$**	**P/R/mAP$_{50}$/ mAP$_{50-95}$**
YOLO12m	0.629/0.725/0.722/ 0.449	0.636/0.637/ 0.681/0.408	0.623/0.813/ 0.763/0.491
YOLO12s (*)	0.580/0.608/0.617/ 0.358	0.514/0.632/ 0.599/0.350	0.646/0.584/ 0.635/0.367
YOLO12s (1)	0.651/0.699/0.729/ 0.452	0.654/0.626/ 0.689/0.419	0.648/0.773/ 0.770/0.486
YOLO12s (2)	0.648/0.710/**0.733**/ **0.458**	0.661/0.629/ 0.696/0.425	0.635/0.791/ 0.770/0.491

(*) Without any augmentations
(1) Uses Config 1 augmentations
(2) Uses Config 2 augmentations
P and R stand for Precision and Recall respectively

Table 3
Training model performance comparison. The * indicates differences in the size of the dataset.

Deformity	P	R	$\mathbf{mAP}_{50}$	$^{mAP}50-95$	Model	Dataset (Train/ Val)
E. seabass pectoral fin	0.723	0.763	0.787	0.538	YOLO8n	483/111
	0.720	0.712	0.759	0.514	YOLO8l	483/111
	0.730	0.625	0.703	0.470	YOLO12s	483/111
	0.779	0.598	0.607	0.402	RT-DETR	483/111
E. seabass caudal fin	0.682	0.607	0.664	0.509	YOLO8l	1288/ 412*
	0.665	0.663	0.711	0.526	YOLO12s	**1718/ 482**
	0.619	0.607	0.587	0.437	RT-DETR	**1718/ 482**
G. seabream pectoral fin	0.504	0.490	0.516	0.307	YOLO8l	701/ 301*
	0.648	0.710	0.733	0.458	YOLO12s	**3604/ 636**
	0.611	0.616	0.600	0.375	RT-DETR	**3604/ 636**
G. seabream caudal fin	0.703	0.776	0.807	0.599	YOLO8l	2041/ 867
	0.708	0.764	0.807	0.604	YOLO12s	2041/ 867
	0.656	0.718	0.686	0.509	RT-DETR	2041/ 867
Red Spot	0.828	0.858	0.885	0.4	YOLO8l	220/72
	0.845	0.877	0.883	0.338	YOLO12s	220/72
	0.901	0.89	0.911	0.377	RT-DETR	220/72

For the European seabass YOLOv8n was the best performing model with $\mathbf{mAP}_{50} = 0.79$.

Regarding the caudal fin, YOLOv12s was the best performing model for both, European seabass ($\mathbf{mAP}_{50} = 0.71$) and gilthead seabream ($\mathbf{mAP}_{50} = 0.81$). Also the difference in the European seabass dataset size could affect the result.

The class-specific analysis revealed a consistent pattern across all models (Table 2): "Good Fin" achieved higher performance across all metrics compared to "Bad Fin". This performance difference is particularly evident in recall values, where "Good Fin" outperforms "Bad Fin" by approximately 16–20 %.

The RT-DETR model only performed equally well with YOLO12s for the red spot, but had worse performance on the rest of the tasks. Table 4 illustrates the best results selected (between the different models tested) for each of the deformity.

In terms of model architecture, the smaller YOLO12s outperformed larger models in most experiments while maintaining faster inference **speeds** (1.8ms/image), compared to YOLO12m (3.6ms/image) demonstrating that parameter efficiency can be achieved without compromising detection performance and making it particularly suitable for real-time underwater detection applications. This efficiency advantage, combined with its smaller memory footprint, highlights the effectiveness of the transformer-based architecture for this specific underwater detection task.

All different model results presented here used the optimal augmentation configuration (Config 2).

Table 4
Best performing models (mAP_{50}).

Deformity	P	R	$\mathbf{mAP}_{50}$	$^{mAP}50-95$	Model	Dataset (Train/ Val)
E. seabass pectoral fin	0.723	0.763	0.787	0.538	YOLO8n	483/111
E. seabass caudal fin	0.665	0.663	0.711	0.526	YOLO12s	1718/ 482
G. seabream pectoral fin	0.648	0.710	0.733	0.458	YOLO12s	2041/ 864
G. seabream caudal fin	0.708	0.764	0.807	0.604	YOLO12s	2041/ 867
Red Spot	0.901	0.89	0.911	0.377	RT-DETR	220/72

4. Discussion

This study demonstrates the feasibility and efficiency of AI-powered deep learning computer vision models for the real-time monitoring of fin deformities, operculum deformities and skin lesions ("red spots") in two economically significant Mediterranean aquaculture species, the European seabass and gilthead seabream, highlighting their potential as practical tools for fish welfare assessment in Mediterranean aquaculture. The proposed approach integrates data acquisition, data augmentation, and annotation optimization with state-of-the-art object detection architectures, including YOLOv8 (Jocher et al., 2023) and the recent YOLOv12 (Tian et al., 2025), and achieves promising detection performance on underwater images collected under real commercial farming conditions.

One of the objectives was to find which model would perform best in terms of accuracy and time. Despite the fewer parameters than its medium-sized counterparts, YOLOv12s was the best performing model, as it showed consistently better results in combination with time and precision. This supports recent findings that smaller, well-optimized architectures can be more effective in constrained real-time environments, such as underwater monitoring (Feng et al., 2024; Yeh et al., 2022; Yan et al., 2024). The model's high inference speed (1.8 ms/image) and low memory footprint further highlight its potential for integration into live monitoring systems in aquaculture facilities.

This study initially employed YOLOv8m and YOLOv8l architectures, following current state-of-the-art approaches for object detection. However, preliminary tests revealed limitations when training these large-scale models on relatively modest datasets of 300–4000 underwater images. The extensive parameter count of these models (43.6 M for YOLOv8l and 25.9 M for YOLOv8m (Ultralytics, 2023) resulted in suboptimal performance, as the dataset provided insufficient samples to effectively train the numerous parameters. This observation aligns with findings from Rosenfeld et al. (2020) regarding the relationship between model capacity and dataset size.

Consequently, we turned to more parameter-efficient architectures, specifically YOLOv12s (Tian et al., 2025) variants. This approach is supported by Wang et al. (2023), who demonstrated that smaller YOLO variants can outperform models with significantly more parameters in certain detection scenarios. Our shift proved particularly advantageous with the recent introduction of YOLOv12 (Tian et al., 2025), which incorporates transformer-based attention mechanisms within a lightweight framework (9.2 M parameters), similar to the approach described by Liu et al. (2021). These smaller models achieved better generalization and avoided overfitting on our limited dataset while maintaining sufficient representational capacity for the underwater detection task, consistent with the findings of Tan and Le (2019). Our experimental results demonstrated this efficiency, with YOLOv12s achieving good performance in the Seabream pectoral fin experiment (mAP_{50} of 0.73) despite having less parameters. It also enables great inference speed, even on low end devices like the Raspberry Pi, compared to larger models.

The annotation sets were affected by the fish species behavior. The two species studied exhibited different behaviors and reactions to the presence of the underwater camera. The gilthead seabream had a positive response to the external stimulus of the camera, compared to the European seabass that kept a distance from the camera, resulting in higher-resolution image data for gilthead seabream. This outcome had a quality effect during the annotation process, as the fish in the camera's

field of view, combined with the good environmental conditions, enabled a larger annotation set to be created for the gilthead seabream in comparison to European seabass.

Another objective was to improve and enhance the annotation dataset to improve model performance. Augmentation significantly improved detection performance. Mosaic and erasing augmentations, in particular, enhanced model performance by simulating realistic occlusions and crowding in underwater environments. The work of Lin et al. (2020) enhances our finding as it showed improvements after investigating different augmentation strategies in overlapping, occluded, and blurred objects in underwater image dataset. In addition, Zhou et al. (2022) also used Mosaic data augmentation (after an image enhancement step) to enrich the dataset with small targets and improve detection robustness in underwater marine biology images. Our results emphasize the importance of tailoring augmentation pipelines to the specific characteristics of the imaging do- main—especially in underwater settings where factors such as lighting, turbidity, and movement introduce significant variability.

Classification performance was generally higher for “Good Fin” examples compared to “Bad Fin”’ ones, as indicated by consistently higher recall and mAP scores across all datasets. This disparity may be partially explained by the greater morphological variability and visual ambiguity inherent in fins with deformities / lesions. “Good Fins” tend to exhibit uniform shapes and textures, whereas “Bad Fins” present a broader spectrum of deformities and lesions, making consistent detection more challenging. Variability issues have been addressed in other studies too (Li et al., 2024; Ouyang et al., 2025). This suggests a need for further refinement in the model’s ability to generalize across diverse deformity types.

The red spot detection task yielded the highest overall metrics, with a precision of 0.85 and mAP50 of 0.88, confirming that skin lesions can be reliably identified through visual cues using relatively lightweight architectures. This task also benefited from the distinct contrast between red spots and surrounding skin, which likely contributed to the model’s high performance. The number of the red spot per each fish could be an interesting parameter to be further considered and incorporated in our tool. The appearance of more than one red spot was very uncommon in our dataset. Enhancing our dataset with more images of multiple red spots per individual and incorporating segmentation and other more advanced computer vision setups, we could be able to quantify the percentage multiple lesions pes individual.

Using a unified modern object detection YOLO-based framework, our work addressed multiple deformities, i.e. fin, operculum and skin using two Mediterranean species, the European seabass and the gilthead seabream under challenging underwater farm conditions. We have not found similar studies that incorporate variable deformity types and multiple species. Other researchers have applied deep learning to detect only one deformity, either fin damage (Ouyang et al., 2025) or skin lesions (Gupta et al., 2022; Yu et al., 2023) in controlled imaging environments and in different aquaculture species.

This work is the first (to our knowledge) to apply transformer-enhanced YOLOv12 with real-time inference for morphological deformities in aquaculture. Moreover, our system is designed for operational farm conditions, where underwater imagery is subject to turbidity, occlusion, and lighting variability, thereby addressing challenges that previous studies have not fully considered.

Despite the encouraging results, the study had several limitations. First, the dataset size, especially for red spot detection and certain fin categories, remained relatively small. However, even with the small sample size, the precision was more than 0.7. Although the annotation pipeline allows for iterative dataset expansion through AI-assisted labeling, model performance would likely improve with larger, more diverse training data covering a broader range of conditions and deformity types. Second, despite the removal of poor-quality images based on defined criteria there are still significant challenges especially in fin classification (that is also a more demanding task) because of motion blur, occlusion, and inconsistent lighting and there should be future improvement.

Another challenge that needs to be addressed is the identity switching and inconsistent labeling when using multi-object tracking, for filtering the detections, despite the fact that we implemented post-processing corrections. We could explore more sophisticated tracking techniques in the future or could try to integrate spatio-temporal models to enhance tracking fidelity in such dynamic underwater environments. Finally, while this study focused on binary classification of fins as "Good" or "Bad," future developments could incorporate a multi-class or severity grading system, enabling more detailed assessments of deformities. Additionally, incorporating 3D reconstruction techniques or using stereo vision data could provide depth cues that further enhance morphological analysis.

Despite certain limitations, this methodology has shown promising results in identifying both fin deformities and skin lesions (red spots) from underwater images captured in real-world farming conditions. Its lightweight characteristics make it a valuable tool for real-time detection of deformities in Mediterranean aquaculture.

This study demonstrates the feasibility and efficiency of real-time, AI-powered computer vision models for the automatic detection and annotation of fin deformities, operculum deformities, and skin lesions (“red spots”) in European seabass and gilthead seabream. The system was designed and validated under commercial aquaculture conditions, enabling continuous, low-cost monitoring at farm scale. By supporting early detection of morphological deformities, the proposed approach enhances fish welfare, improves health management, and provides a practical solution for operational decision-making in modern aquaculture.

CRediT authorship contribution statement

Ioannis Christofilogiannis: Writing – original draft, Software, Methodology, Formal analysis, Data curation. **Dimitra G. Georgopoulou:** Writing – original draft, Supervision, Methodology, Data curation. **Charalabos Vouidaskis:** Writing – review & editing, Software, Methodology, Investigation, Formal analysis, Data curation. **Zacharias Choulakis:** Writing – review & editing, Software, Methodology, Investigation, Data curation. **Dimitris Voskakis:** Writing – review & editing, Supervision, Software, Methodology, Data curation, Conceptualization. **Nikos Papandroulakis:** Writing – review & editing, Supervision, Resources, Project administration, Funding acquisition, Conceptualization.

Data/Code availability Future Work

The AI assisted annotation tool is available openly on GitHub (https://github.com/christofilojohn/YOLO-Annotation-Tool). The aim of the tool is to leverage pre-trained YOLO models for further annotations. Even though this tool was developed for the classification problem of pectoral and caudal fins, it can generalize to other binary classification problems. It’s an easy to use tool built using Python and can be utilized by end users without much technical knowledge.

Declaration of Generative AI and AI-assisted technologies in the writing process

During the preparation of this work the author(s) used ChatGPT in order to improve the readability of the draft manuscript. During the preparation of this work the authors used Claude 3.5 for debugging of the Assisted Annotation tool. After using these tools, the authors reviewed and edited the content as needed and take full responsibility for the content of the published article.

Declaration of Competing Interest

The authors declare that they have no known competing financial

interests or personal relationships that could have appeared to influence the work reported in this paper.

Acknowledgments

The authors would like to thank all the internship students that helped with the annotation of the dataset.

Appendix

The figures with the different categories of pectoral and caudal fins deformities and lesions as well as the skin red spots were based on actual selected underwater camera images of European seabass and gilthead seabream from real fish farm environment. (Fig. A1).

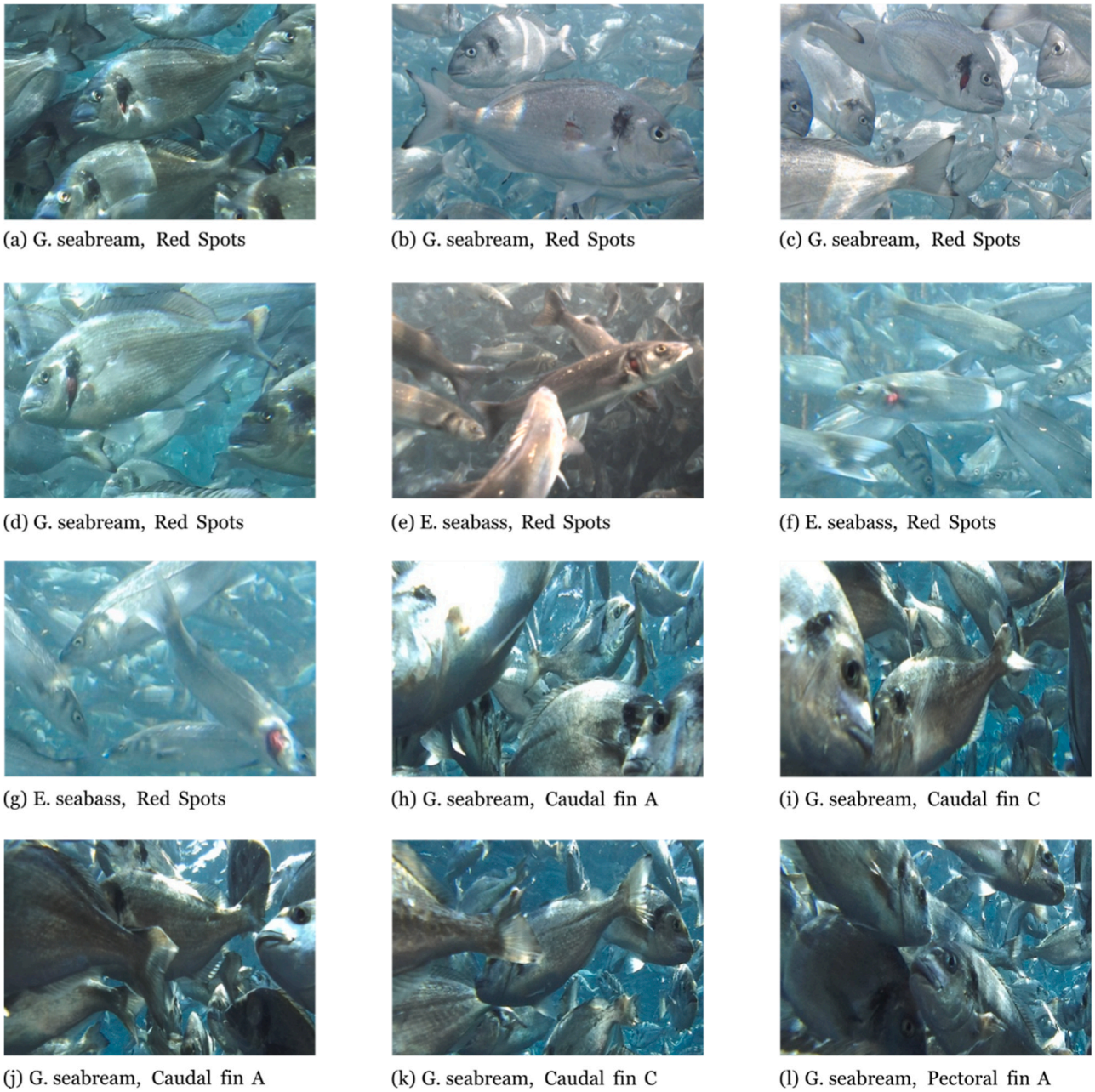

Fig. A1. Sample dataset images showing various deformities / lesions. In the caption of each image is the fish species name and the corresponding deformity / lesion category

(a) G. seabream, Pectoral fin D

(b) G. seabream, Pectoral fin D

(c) G. seabream, Pectoral fin E

(d) G. seabream, Caudal fin B

(e) G. seabream, Caudal fin B

(f) G. seabream, Pectoral fin C

(g) G. seabream, Caudal fin B

(h) G. seabream, Pectoral fin C

(i) G. seabream, Pectoral fin C

(j) G. seabream, Pectoral fin C

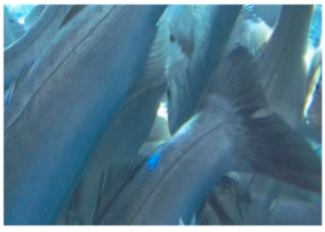

(k) E. seabass, Caudal fin A

(l) E. seabass, Caudal fin B

(m) E. seabass, Caudal fin C

(n) E. seabass, Caudal fin C

(o) E. seabass, Caudal fin B

(p) E. seabass, Caudal fin C

(q) E. seabass, Pectoral fin B

(r) E. seabass, Pectoral fin A

Fig. A2. Sample dataset images showing various deformities / lesions. In the caption of each image is the fish species name and the corresponding deformity / lesion category

Data availability

Data will be made available on request.

References

Bellis, G., Papaggelos, P., Vlachogianni, E., Laleas, I., Moustos, S., Patas, T., Poulios, S., Tzioumakis, N., Giakas, G., Bokas, D., Kokkotis, C., Tsaopoulos, D., 2024. Automated sorting system for skeletal deformities in cultured fishes. URL: https://www.mdpi.com/2504-3900/94/1/58 Proceedings 94. https://doi.org/10.3390/proceedings2024094058.

Beraldo, P., Pinosa, M., Tibaldi, E., Canavese, B., 2003. Abnormalities of the operculum in gilthead sea bream (Sparus aurata): morphological description. Aquaculture 220 (1-4), 89–99.

Boglione, C., Gisbert, E., Gavaia, P., E. Witten, P., Moren, M., Fontagné, S., Koumoundouros, G., 2013. Skeletal anomalies in reared European fish larvae and juveniles. Part 2: main typologies, occurrences and causative factors. Rev. Aquac. 5, S121–S167.

Boglione, C., Pulcini, D., Scardi, M., Palamara, E., Russo, T., Cataudella, S., 2014. Skeletal anomaly monitoring in rainbow trout (*Oncorhynchus mykiss*, Walbaum 1792) reared under different conditions. PLoS One 9, e96983.

Branson, E.J., 2008. Fish welfare. John Wiley & Sons.

Čapek, D., Safroshkin, M., Morales-Navarrete, H., Toulany, N., Arutyunov, G., Kurzbach, A., Bihler, J., Hagauer, J., Kick, S., Jones, F., et al., 2023. Embryonet: using deep learning to link embryonic phenotypes to signaling pathways. Nat. Methods 20, 815–823.

Chandra, G., Saini, V., Kumar, S., Fopp-Bayat, D., 2024. Deformities in fish: A barrier for responsible aquaculture and sustainable fisheries. Rev. Aquac. 16, 872–891.

Costa, C., Antonucci, F., Boglione, C., Menesatti, P., Vandeputte, M., Chatain, B., 2013. Automated sorting for size, sex and skeletal anomalies of cultured seabass using external shape analysis. URL: https://www.sciencedirect.com/science/article/pii/S0144860912000659 Aquac. Eng. 52, 58–64. https://doi.org/10.1016/j.aquaeng.2012.09.001.

Cuvier, G., Valenciennes, M., 1828. Histoire naturelle des poissons. volume color plates. Chez F. G. Levrault, Paris, pp. 141–255. ⟨https://archive.org/details/histoirenaturell141255cuvi/page/n13/mode/2up⟩. accessed via Inter- net Archive: May 2025.

Divanach, P., Boglione, C., Menu, B., Koumoundouros, G., Kentouri, M., Cataudella, S., et al., 1996. Abnormalities in finfish mariculture: An overview of the problem, causes and solutions. Spec. Publ. /Eur. Aquac. Soc. 45–66.

Dygut, J., Piwowar, M., 2025. Distinction Between Dysplasia, Malformation, and Deformity-Towards the Proper Diagnosis and Treatment of Hip Development Disorders. Diagn. (Basel) 15 (12), 1547. https://doi.org/10.3390/diagnostics15121547. PMID: 40564867; PMCID: PMC12191916.

FAO, 2024. The State of World Fisheries and Aquaculture 2024 - Blue Transformation in action. FAO, Rome. https://doi.org/10.4060/cd0683en.

Feng, D., Liu, H., Wu, L., Ying, X., Qu, X., Gao, Y., Gui, F., Zhou, C., 2025. Morphological feature assessment of Larimichthys crocea for quality grading: a computer vision approach. Aquac. Int. 33, 384.

Feng, G., Xiong, Z., Pang, H., Gao, Y., Zhang, Z., Yang, J., Ma, Z., 2024. Rtl-yolov8n: A lightweight model for efficient and accurate underwater tar- get detection. URL: https://www.mdpi.com/2410-3888/9/8/294 Fishes 9. https://doi.org/10.3390/fishes9080294.

Flüchter, J., 1979. Identification and treatment of diseases in the common sole (*Solea solea* l.). Aquaculture 16, 271–274.

Gourzioti, E., Kolygas, M., Athanasopoulou, F., Babilli, V., 2018. Tenacibaculosis in aquaculture farmed marine fish. J. Hell. Vet. Med. Soc. 67, 21. https://doi.org/10.12681/jhvms.15620.

Gupta, A., Bringsdal, E., Knausgård, K.M., Goodwin, M., 2022. Accurate wound and lice detection in atlantic salmon fish using a convolutional neural network. Fishes 7, 345.

HAPO, 2025. Aquaculture Annual Report. Technical Report. Hellenic Aquaculture Producers Organisation.

Hatziathanasiou, A., Paspatis, M., Houbart, M., Kestemont, P., Stefanakis, S., Kentouri, M., 2002. Survival, growth and feeding in early life stages of European seabass (*Dicentrarchus labrax*) intensively cultured under different stocking densities. Aquaculture 205, 89–102. https://doi.org/10.1016/S0044-8486(01)00672-X.

Hennekam, R., Biesecker, L., Allanson, J., et al., 2013. Elements of morphology: general terms for congenital anomalies. Am. J. Med Genet A 161A, 2726–2733. https://doi.org/10.1002/ajmg.a.36249.

Holm, H., Ytteborg, E., Høst, V., Reed, A.K., Dalum, A.S., Bæverfjord, G., 2020. A pathomorphological description of cross-stitch vertebrae in farmed at- lantic salmon (*Salmo salar* l.). URL: https://www.sciencedirect.com/science/article/pii/S0044848620302295 Aquaculture 526, 735382. https://doi.org/10.1016/j.aquaculture.2020.735382.

Jeannine, P., Bayon, N., 2009. Effects of temperature, stocking density and farming conditions on fin damage in European seabass (*Dicentrarchus labrax*). In: Aquatic living resources (0990-7440), 22. EDP Sciences, pp. 349–362. https://doi.org/10.1051/alr/2009047, 2009-07.

Jocher, G., Chaurasia, A., Qiu, J., 2023. Ultra yolov8. ⟨https://github.com/ultralytics/ultralytics⟩ (URL:).

Koumoundouros, G., 2010. Morpho-anatomical abnormalities in mediterranean marine aquaculture. Recent Adv. Aquac. Res. 661, 125–148.

Koumoundouros, G., Oran, G., Divanach, P., Stefanakis, S., Kentouri, M., 1997. The opercular complex deformity in intensive gilthead seabream (*Sparus aurata* l.) larviculture. moment of apparition and description. Aquaculture 156, 165–177.

Kumar, N., Marée, R., Geurts, P., Muller, M., 2023. Recent advances in bioimage analysis methods for detecting skeletal deformities in biomedical and aquaculture fish species. Biomolecules 13, 1797. ⟨https://www.overleaf.com/project/68c287a620e2073ae3b80814⟩.

Kvæstad, B., Hansen, B.H., Davies, E., 2022. Automated morphometrics on mi- croscopy images of atlantic cod larvae using mask r-cnn and classical machine vision techniques. MethodsX 9, 101598.

Lauder, G.V., 2000. Function of the caudal fin during locomotion in fishes: kinematics, flow visualization, and evolutionary patterns. Am. Zool. 40, 101–122.

Lévesque, M., Feng, Y., Jones, R.A., Martin, P., 2013. Inflammation drives wound hyperpigmentation in zebrafish by recruiting pigment cells to sites of tissue damage. Dis. Models Mech. 6, 508–515.

Li, D., Li, X., Wang, Q., Hao, Y., 2022. Advanced techniques for the intelligent diagnosis of fish diseases: A review. Animals 12, 2938.

Li, X., Zhao, S., Chen, C., Cui, H., Li, D., Zhao, R., 2024. Yolo-fd: An accurate fish disease detection method based on multi-task learning. Expert Syst. Appl. 258, 125085.

Lin, W.H., Zhong, J.X., Liu, S., Li, T., Li, G., 2020. Roimix Propos. Fusion Mult. Images Underw. Object Detect. ⟨https://arxiv.org/abs/1911.03029⟩ arXiv:1911.03029.

Liu, C., Wang, Z., Li, Y., Zhang, Z., Li, J., Xu, C., Du, R., Li, D., Duan, Q., 2023. Research progress of computer vision technology in abnormal fish detection. Aquac. Eng. 103, 102350.

Liu, Z., Lin, Y., Cao, Y., Hu, H., Wei, Y., Zhang, Z., Lin, S., Guo, B., 2021. Swin transformer: Hierarchical vision transformer using shifted windows. In: Proceedings of the IEEE/CVF international conference on computer vision, pp. 10012–10022.

Loshchilov, I., Hutter, F., 2017. Decoupled Weight Decay Regul. arXiv Prepr. arXiv 1711, 05101.

Luo, D., 2024. Quantitative analysis of fish morphology through landmark and outline-based geometric morphometrics with free software. BioProtoc. 14, e5087.

Mhalhel, K., Levanti, M., Abbate, F., Laurà, R., Guerrera, M.C., Aragona, M., Porcino, C., Pansera, L., Sicari, M., Cometa, M., et al., 2023. Skeletal morphogenesis and anomalies in gilthead seabream: A comprehensive review. Int. J. Mol. Sci. 24, 16030.

Naudin, S., Pella, H., Charlon, N., Garric, J., Bergot, P., 1996. Détection de larves de poisson anormales par analyse d'images. Aquat. Living Resour. 9, 281–287.

Nikolakakis, S., Bossier, P., Kanlis, G., Dierckens, K., Adriaens, D., 2014. Protocol for quantitative shape analysis of deformities in early larval european seabass Dicentrarchus labrax. J. Fish. Biol. 84, 206–224.

Noble, C., Cañon Jones, H.A., Damsgård, B., Flood, M.J., Midling, K.Ø., Roque, A., Sæther, B.S., Cottee, S.Y., 2012. Injuries and deformities in fish: their potential impacts upon aquacultural production and welfare. Fish. Physiol. Biochem. 38, 61–83.

Noble, C., Abbink, W., Alvestad, R., Ardó, L., Bégout, M.L., Bloecher, N., Burgerhout, E., Calduch-Giner, J., Chivite-Alcalde, M., Císař, P., Durland, E., et al., 2026. Welfare Indicators for Aquaculture Research: Toolboxes for Five Farmed European Fish Species. Rev. Aquac. 18 (1), e70109.

Ouyang, C., Peng, H., Tan, M., Yang, L., Deng, J., Jiang, P., Hu, W., Wang, Y., 2025. Yolo-tps: A multi-module synergistic high-precision fish-disease detection model for complex aquaculture environments. Animals 15, 2356.

Paperna, I., Ross, B., Colorni, A., Colorni, B., 1980. Diseases of marine fish cultured in Eilat mariculture project based at the Gulf of Aqaba, Red Sea. Stud. Rev. Gen. Fish. Counc. Mediterr. (FAO) (57).

Pousis, C., Di Comite, M., Zupa, R., Passantino, L., Hala, E., Corriero, A., 2022. Microradiography as a useful technique for the rapid detection of skeletal anomalies in early seabream juveniles. J. Fish. Dis. 45, 1237.

Rizgalla, J., Bron, J., Shinn, A., Herath, T., Paladini, G., Ferguson, H., 2016. Ulcerative dermatitis in wild dusky grouper Epinephelus marginatus (lowe) from libyan waters. J. Fish. Dis. 39, 1457–1466.

Rosenfeld, J.S., Rosenfeld, A., Belinkov, Y., Shavit, N., 2020. A constructive prediction of the generalization error across scales. arXiv preprint arXiv:2001.02114.

Saleh, A., Jones, D., Jerry, D., Azghadi, M.R., 2023. Mfld-net: a lightweight deep learning network for fish morphometry using landmark detection. Aquat. Ecol. 57, 913–931.

Schmidt, J.G., Thompson, K., Padros, F., 2018. Emerging skin diseases in aquaculture. Bull. Eur. Assoc. Fish. Pathol. 38, 122–129.

Seafish, 2025. European sea bass: Aquaculture profile. ⟨https://www.seafish.org/responsible-sourcing/aquaculture-farming-seafood/species-farmed-in-aquaculture/aquaculture-profiles/european-sea-bass/⟩. accessed May 2025.

Smith, S.B., Donahue, A.P., Lipkin, R.J., Blazer, V., Schmitt, C.J., Goede, R.W., 2002. Illustrated field guide for assessing external and internal anomalies in fish. Technical Report. US Geological Survey.

Sun, P.L., Hawkins, W.E., Overstreet, R.M., Brown-Peterson, N.J., 2009. Morphological deformities as biomarkers in fish from contaminated rivers in Taiwan. Int. J. Environ. Res. Public Health 6, 2307–2331.

Sveen, L., Karlsen, C., Ytteborg, E., 2020. Mechanical induced wounds in fish a review on models and healing mechanisms. Rev. Aquac. 12, 2446–2465. https://doi.org/10.1111/raq.12443.

Tan, M., Le, Q., 2019. Efficientnet: Rethinking model scaling for convolutional neural networks. In: International conference on machine learning. PMLR, pp. 6105–6114.

Teixidó Condomines, E., Kießling, T.R., Krupp, E., Quevedo, C., Muriana, A., Scholz, S., 2019. Automated morphological feature assessment for zebrafish embryo developmental toxicity screens. Toxicol. Sci. 167 (num. 2), 438–449, 2019.

Thorsen, D.H., Westneat, M.W., 2005. Diversity of pectoral fin structure and function in fishes with labriform propulsion. J. Morphol. 263, 133–150.

Tian, Y., Ye, Q., Doermann, D., 2025. Yolov12: Attention-centric real-time object detectors. arXiv preprint arXiv:2502.12524.

Ultralytics, 2023. Yolov8: A high performance object detection model. GitHub repository. URL: ⟨https://github.com/ultralytics/ultralytics⟩.

Verhaegen, Y., Adriaens, D., De Wolf, T., Dhert, P., Sorgeloos, P., 2007. Deformities in larval gilthead sea bream (*Sparus aurata*): A qualitative and quantitative analysis using geometric morphometrics. Aquaculture 268 (1-4), 156–168.

Voskakis, D., Makris, A., Papandroulakis, N., 2021. Deep learning based fish length estimation. An application for the Mediterranean aquaculture (September). OCEANS 2021: San Diego–porto. IEEE, pp. 1–5 (September).

Wang, C.Y., Bochkovskiy, A., Liao, H.Y.M., 2023. Yolov7: Trainable bag-of-freebies sets new state-of-the-art for real-time object detectors. Proc. IEEE/CVF Conf. Comput. Vis. Pattern Recognit. 7464–7475.

Westneat, M.W., Thorsen, D.H., Walker, J.A., Hale, M.E., 2004. Structure, function, and neural control of pectoral fins in fishes. IEEE J. Ocean. Eng. 29, 674–683.

Yan, C., Yan, S., Yao, T., Yu, Y., Pan, G., Liu, L., Wang, M., Bai, J., 2024. A lightweight network based on multi-scale asymmetric convolutional neural networks with attention mechanism for ship-radiated noise classification. J. Mar. Sci. Eng. 12, 130.

Yeh, C.H., Lin, C.H., Kang, L.W., Huang, C.H., Lin, M.H., Chang, C.Y., Wang, C.C., 2022. Lightweight deep neural network for joint learning of underwater object detection and color conversion. IEEE Trans. Neural Netw. Learn. Syst. 33, 6129–6143. https://doi.org/10.1109/TNNLS.2021.3072414.

Yu, C., Hu, Z., Han, B., Wang, P., Zhao, Y., Wu, H., 2021. Intelligent measurement of morphological characteristics of fish using improved u-net. Electronics 10, 1426.

Yu, G., Zhang, J., Chen, A., Wan, R., 2023. Detection and identification of fish skin health status referring to four common diseases based on improved yolov4 model. Fishes 8, 186.

Yun, T., Shin, S., Bang, K., Lee, M., Cho, J.A., Baek, M., 2021. Skin wound healing rate in fish depends on species and microbiota. Int. J. Mol. Sci. 22, 7804.

Zhao, Y., Lv, W., Xu, S., Wei, J., Wang, G., Dang, Q., Liu, Y., Chen, J., 2024. Detrs beat yolos Real. Time Object Detect. 08069. ⟨https://arxiv.org/abs/2304⟩. arXiv: 2304.08069.

Zhou, J., Yang, Q., Meng, H., Gao, D., 2022. An underwater target recognition method based on improved yolov4 in complex marine environment. Syst. Sci. Control Eng. 10, 590–602.